View metadata, citation and similar papers at core.ac.uk
brought to you by CORE
provided by Woods Hole Open Access Server

Laboratory Experiments on the Interaction of a Buoyant Coastal Current with a Canyon: Application to the East Greenland Current

DAVID A. SUTHERLAND

MIT/WHOI Joint Program, Woods Hole, Massachusetts

CLAUDIA CENEDESE

Department of Physical Oceanography, Woods Hole Oceanographic Institution, Woods Hole, Massachusetts

(Manuscript received 11 April 2008, in final form 3 December 2008)

ABSTRACT

This paper presents a set of laboratory experiments focused on how a buoyant coastal current flowing over a sloping bottom interacts with a canyon and what controls the separation, if any, of the current from the upstream canyon bend. The results show that the separation of a buoyant coastal current depends on the current width W relative to the radius of curvature of the bathymetry ρ_c. The flow moved across the mouth of the canyon (i.e., separated) for $W/\rho_c > 1$, in agreement with previous results. The present study extends previous work by examining both slope-controlled and surface-trapped currents, and using a geometry specific to investigating buoyant current–canyon interaction. The authors find that, although bottom friction is important in setting the position of the buoyant front, the separation process driven by the inertia of the flow could overcome even the strongest bathymetric influence. Application of the laboratory results to the East Greenland Current (EGC), an Arctic-origin buoyant current that is observed to flow in two branches south of Denmark Strait, suggests that the path of the EGC is influenced by the large canyons cutting across the shelf, as the range of W/ρ_c in the ocean spans those observed in the laboratory. What causes the formation of a two-branched EGC structure downstream of the Kangerdlugssuaq Canyon (~68°N, 32°W) is still unclear, but potential mechanisms are discussed.

1. Introduction

Exiting the Arctic Ocean through western Fram Strait, the East Greenland Current (EGC) brings water of polar origin equatorward along the east coast of Greenland. South of Denmark Strait (Fig. 1), the relatively warm and salty Irminger Current (IC) merges with the EGC on its offshore side, while inshore a separate branch of the EGC, the East Greenland Coastal Current (EGCC), is found (Pickart et al. 2005), although its origin and dynamics are still not completely understood. The shelf bathymetry off southeast Greenland is highly variable, narrowing in width dramatically from north to south and cut by numerous large-scale canyons and basins. One such canyon (width ~50 km), the Kangerdlugssuaq Trough (KG) (Fig. 1), crosses the entire shelf with depths up to 600 m, while typical shelf depths are ~250 m in this area. The goal of this study is to focus on the interaction of a buoyant current with a canyon, which influences the pathway of buoyant coastal currents such as the EGC. Since observations are scarce inshore of the shelf break, we rely on a set of idealized laboratory experiments to model the process of a buoyant flow encountering a canyon. Note that we use the terms *buoyant flow*, *buoyant current*, and *coastal current* interchangeably throughout the paper.

Numerous laboratory and numerical experiments have investigated the dynamics of buoyant currents. Notably, Lentz and Helfrich (2002) described the basic scaling of a coastal current flowing along a sloping bottom in the laboratory and successfully compared their results to observations representative of Delaware Bay and to previous theory (Chapman and Lentz 1994; Yankovsky and Chapman 1997).

The presence of a sloping bottom has a stabilizing effect on coastal currents. Laboratory experiments on coastal currents flowing over a sloping bottom tend to

Corresponding author address: David A. Sutherland, University of Washington, School of Oceanography, Box 355351, Seattle, WA 98195.
E-mail: dsuth@u.washington.edu

DOI: 10.1175/2008JPO4028.1

© 2009 American Meteorological Society

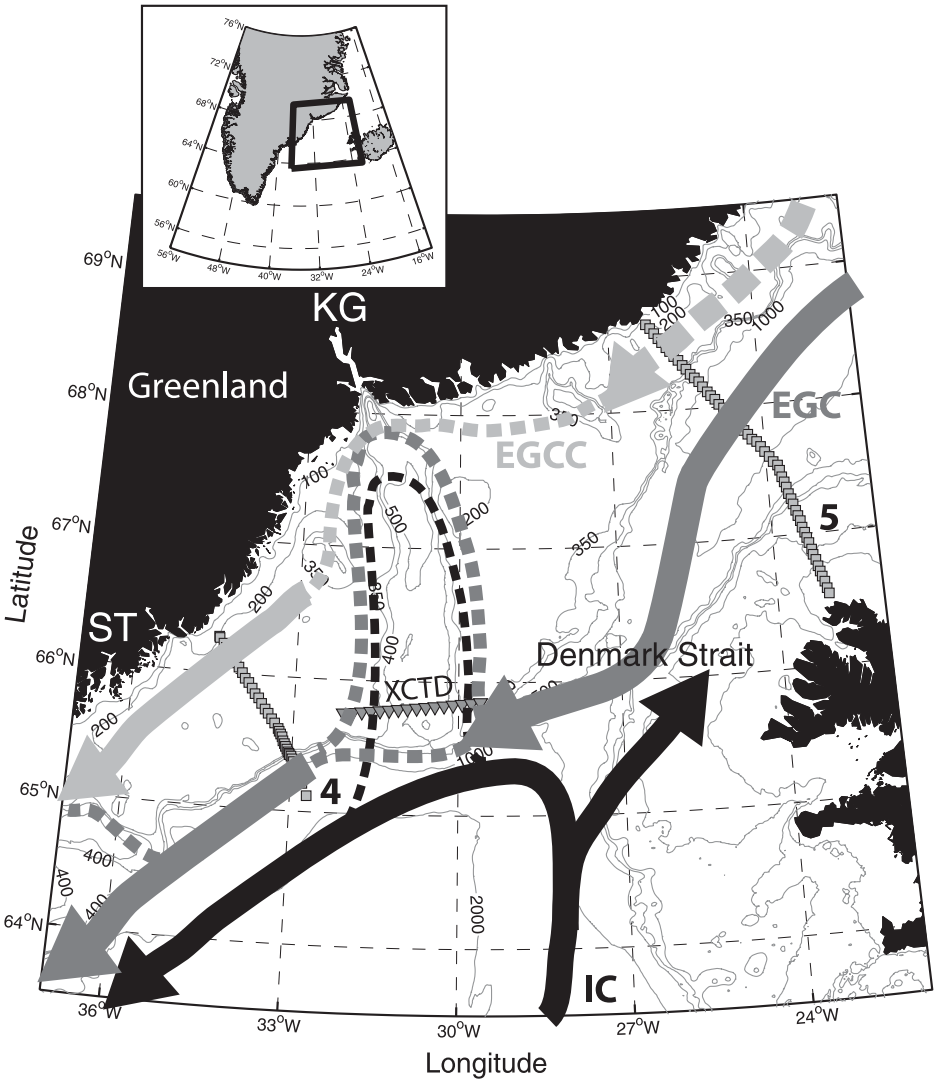

FIG. 1. Schematic of the major circulation patterns near the Kangerdlugssuaq Trough (KG) region off east Greenland. Dashed lines indicate possible flow paths of the East Greenland Current (EGC) and the East Greenland Coastal Current (EGCC), while solid lines display observed positions of the EGCC, EGC, and Irminger Current (IC). Selected isobaths from the GEBCO bathymetry dataset (BODC et al. 2003) illustrate the trough region of the KG and the Sermilik Trough (ST). Gray symbols indicate the position of hydrographic stations along sections 4 and 5 taken in 2004, and XCTD labels the 2002 transect.

meander and form eddies less than their vertical wall counterparts and they more closely resemble oceanic flows (Griffiths and Linden 1981; Cenedese and Linden 2002). Wolfe and Cenedese (2006) recently explored the stability of a coastal current encountering a bathymetric gap with vertical walls between two sloping bottoms. They found that eddies formed within the gap when its width exceeded eight times the internal Rossby radius of deformation of the current but that these disturbances never propagated onto the sloping bathymetry downstream of the gap.

The importance of the width scale of the buoyant flow relative to the scale of the bathymetry has been shown previously as well. Flow separation was found to occur at a bathymetric bend (e.g., a cape) when the radius of curvature of the bathymetry was roughly equal to or less than the inertial radius of the current, u/f, where u is a velocity scale for the flow and f is the Coriolis parameter (e.g., Whitehead and Miller 1979; Bormans and Garrett 1989). This separation was suggested to be the generation mechanism for gyres observed in the Alboran Sea. If no separation occurred, a coastal current trapped to

the shore formed and the gyre disappeared. A similar criterion was found to hold for waters that have been observed to cross from the Scotian Shelf to Georges Bank, with no separation occurring if the density difference across the front was too small (Cho et al. 2002). These results are in agreement with the behavior of a reduced-gravity, inviscid model of a baroclinic current encountering a cape (Klinger 1994a), with separation occurring when $u/f > 0.9\rho_c$, where ρ_c is the radius of curvature of the cape. These studies provide a context for understanding how the EGC interacts with a canyon, but none included a sloping bottom and, consequently, the role that bottom friction might play in influencing the separation process.

A set of revealing numerical model experiments that included bottom friction showed that for certain strengths of the buoyant inflow a surface flow separated from a bathymetric bend and moved across the mouth of a canyon, reattaching to the shelf/slope on the downstream side (Chapman 2003, hereafter DC03). When the density difference was reduced and the flow became slower and narrower, the current remained tied to the bathymetry and traveled into and back out of the canyon with no flow across it. However, the model results were sensitive to an imposed background flow: Separation always occurred when no background flow was present.

The results and discussion presented here extend those of DC03 in a laboratory setting, where no imposed background current is needed to ensure the downstream propagation of the buoyant flow. In addition, the present study spans a wider range of buoyant current scenarios, that is, both slope-controlled and surface-trapped flows, as well as utilizing a more realistic bottom bathymetry than previous laboratory studies.

Finally, the results of this work suggest some potential mechanisms for the formation of the EGCC (Bacon et al. 2002; Sutherland and Pickart 2008) as a distinct flow separate from the EGC. First thought to be a purely meltwater-driven current, recent evidence shows that the EGCC has similar water mass characteristics as the EGC (Sutherland and Pickart 2008), as well as a significant Pacific water signal (Sutherland et al. 2008, manuscript submitted to *J. Geophys. Res.*; Bacon et al. 2008), both of which imply that it is mainly a branch of the EGC.

We briefly review the scaling for buoyant currents on a slope and their interaction with topography in section 2, before discussing our results in sections 3 and 4. The findings from the laboratory are then applied to observational data in section 5 to understand what controls the separation of the EGC near the KG canyon region, and the implications of this process for the EGCC.

2. Buoyant current scaling and theory

a. Review of scaling for a buoyant current on a slope

The dynamics of a buoyant current flowing over a slope far from the source region are relatively well understood. Buoyant currents are commonly assumed to be in geostrophic balance in the cross-shelf direction, with a density front separating the lighter onshore water from the denser offshore water (e.g., Chapman and Lentz 1994; Lentz and Helfrich 2002). Given sufficient time and distance, the current front is advected across the shelf by a bottom Ekman layer velocity that is directed offshore. The front is eventually trapped at a location where the thermal wind shear causes a reversal in the bottom boundary-layer velocity, stopping the advection of the front across the shelf. This trapping depth, h_p, is given by

$$h_p = \sqrt{2Qf/g'} \tag{1}$$

and was tested successfully in models for many different parameter values (Chapman and Lentz 1994; Yankovsky and Chapman 1997). Once the vertical scale of the buoyant current is set by h_p, two horizontal scales follow (Fig. 2). The first, W_b, is the distance from the coast to the trapping depth and equals

$$W_b = h_p/s, \tag{2}$$

where s is the bathymetric slope. The second, W_d, is the internal Rossby radius of deformation and is the natural scale for the width of the density front, given by

$$W_d = \sqrt{g'h_p}/f. \tag{3}$$

The total width of the flow is $W = W_b + W_d$ and compares well to widths observed in the laboratory. This scale can also be written in terms of two wave speeds: $c_w = (g'h_p)^{1/2}$, the internal gravity wave speed, and $c_\alpha = sg'/f$, the phase speed of a long topographic wave, as $W = (c_w/f)(1 + c_w/c_\alpha)$ (Lentz and Helfrich 2002).

To quantify to what degree a buoyant current is tied to the bottom, two limits have been introduced: in the ''slope-controlled'' case, bottom friction is more important, while the current is less coupled to the bottom in the ''surface-trapped'' case. Lentz and Helfrich (2002) define these limits using the ratio c_w/c_α. For $c_w/c_\alpha \ll 1$, the current is surface trapped and its width is W_d, while for $c_w/c_\alpha \gg 1$, the flow is slope controlled and the total width W is a more appropriate horizontal scale.

The velocity of the flow also depends on the degree to which it is slope controlled. Over a sloping bottom, the velocity scale for a buoyant current is

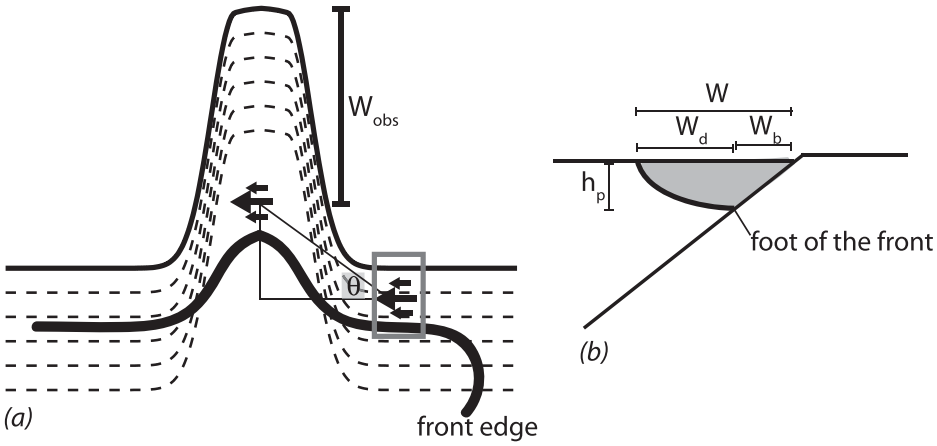

FIG. 2. Schematic showing the variables used to quantify the buoyant current behavior. The edge of the front (heavy line) marks the offshore extent of the current, W_{obs} is the distance from the head of the canyon to the maximum current velocity, while θ is defined as the front angle. The gray box outlines the region where u_{obs} was calculated. (b) Schematic of vertical section through the current showing the depth and width scales defined in the text. Flow is into the page.

$$c_p \approx c_w(1 + c_w/c_\alpha)^{-1}. \quad (4)$$

This velocity scale is called the propagation speed and is always less than c_w, though it approaches that limit in the case of surface-trapped flow (Lentz and Helfrich 2002).

Observations from oceanic flows support this dynamical framework. For example, the depth and width scales of the Chesapeake Bay coastal current were shown to agree well with these theoretical predictions, even in strongly forced regions where both downwelling- and upwelling-favorable winds were common (Lentz and Largier 2006).

b. Review of buoyant current separation scaling

The problem of how a buoyant current separates from a bathymetric bend, such as at a canyon or a cape, has been addressed in the past analytically, numerically, and experimentally with several important scales found that are useful for comparison between the different studies. These include the radius of curvature of the bathymetric bend, ρ_c, which in the present experiments is ~6 cm at the surface, and the inertial radius of the current, u/f. Several studies have found that flow separation occurs at the upstream edge of a bathymetric feature when ρ_c is less than or equal to u/f (Bormans and Garrett 1989; Klinger 1994a; Cho et al. 2002). Garrett (1995) extended the theory to include a sloping bottom but found that, for almost all realistic bottom slopes, the behavior of the separating current remained relatively unchanged, with $u/f\rho_c > 1$ still the applicable criterion.

In the laboratory, the current speed can be scaled by c_p (4) so that u/f is equivalent to W_d (3) for surface-trapped flows only (Lentz and Helfrich 2002). This is equivalent to stating that the flow has a Froude number [$\mathrm{Fr} = u/(g'h_p)^{1/2}$] equal to 1. Hence, for a surface-trapped current, separation is predicted to occur for $W_d/\rho_c > 1$.

Another important scale is the width of the bathymetric feature, whose ratio with W_d (3) was found to influence the stability of a buoyant current as it encountered a bathymetric gap in the laboratory (Wolfe and Cenedese 2006). Other experiments looking at a buoyant current encountering a step change in bathymetry have shown that the incident flow can split at the depth change with part of the flow moving on to the shallower bathymetry, while the rest of the flow continues to follow a constant-depth isobath (Cenedese et al. 2005). However, those experiments focused on different geometries (i.e., a vertical gap and a step) than the one used in the present study.

The width scale of the current relative to the width of the canyon can be defined as a Burger number, $\mathrm{Bu} = W/W_c$, a parameter shown to control cross-shelf exchange in several numerical studies of barotropic flow past a canyon (e.g., Klinck 1996; She and Klinck 2000; Allen et al. 2003). Wide canyons (Bu = 0.82) caused a distortion of the flow but little cross-shelf exchange, while narrow canyons (Bu = 3.3) induced strong vertical motion inside the canyon (Klinck 1996). Furthermore, numerical experiments on barotropic current interaction with cross-shelf topography (Williams et al. 2001) showed that the flow behavior depended on the depth scale of the canyon relative to the ambient shelf depth and the width scale of the sloping bathymetry. For larger features, they found that the flow followed isobaths, while for smaller depth changes the flow tended

to cross the channel bathymetry. In a related study, Sheremet and Kuehl (2007) found a hysteresis in the behavior of a barotropic current encountering a gap, where separation depended on the previous conditions of the flow field.

The numerical experiments of DC03, introduced above, are a primary motivation for the present work, as well as the closest analog to the buoyant current system off Greenland. DC03's motivation was to explain the loss of transport in the boundary current system from the Labrador Shelf to the Middle Atlantic Bight. DC03 hypothesized that these transport losses occurred at a few specific locations along the buoyant current's path, particularly at bathymetric features such as canyons and capes that would allow offshore leakage. The main conclusion of DC03 was that the separation process depended critically on the strength of the buoyant flow compared to the ambient current.

TABLE 1. Variables used in the laboratory experiments. The first three, f, g', and Q, are set a priori and are the Coriolis parameter, reduced gravity, and buoyant water flow rate, respectively. The scales h_p and W_d are calculated from these variables (see text).

Run	f (s^{-1})	g' (cm s^{-2})	Q (cm^3 s^{-1})	h_p (cm)	W_d (cm)	Case*
1	2.5	10	10	2.2	1.9	A
2	0.5	10	10	1.0	6.3	C
3	2.5	20	10	1.6	2.2	A
4	0.5	20	10	0.7	7.5	C
5	1.0	10	10	1.4	3.7	B
6	2.0	10	10	2.0	2.2	A
7	1.75	10	10	1.9	2.5	A
8	1.25	10	10	1.6	3.2	B
9	1.75	20	10	1.3	2.9	A
10	2.5	23	23	2.2	2.9	B
11	2.5	4	4	2.2	1.2	A
12	1.75	14	20	2.2	3.2	B
13	1.89	10	13.25	2.2	2.5	B
14	1.17	6.43	13.46	2.2	3.2	B

* Case refers to the three regimes of steady-state-flow behavior observed in the laboratory, described in detail in section 4 and Fig. 7.

3. Experimental methods

a. Setup

All experiments were conducted in a clear, round, Plexiglas tank of 1-m diameter on a rotating, direct-drive turntable with a vertical axis of rotation. Rotation, reported here as $f = 2\Omega$, where Ω is the rotation rate, was counterclockwise in all runs and varied between 0.5 and 2.5 s^{-1}. A total of 14 experiments were performed with values for the variables of each separate run listed in Table 1.

An idealized bathymetry was constructed from hard foam and placed in the tank (weights placed on top of the foam kept it in place) with one side flush against the wall (Fig. 3). The height of the bathymetry was $H = 20$ cm and the tank was filled to ~18 cm in each experiment. The parameters that describe the shape of the bathymetry—which include the slope $s = \tan\alpha$, the width of the canyon mouth W_c, the length of the canyon L_c, and the radius of curvature ρ_c—were set to be nondimensionally similar to those in previous studies and the KG region shown in Fig. 1. The slope changes from $s = 0.7$ at line a to $s = 3.3$ along the canyon wall to $s = 0.7$ along line b at the head of the canyon. Here $W_c = 25$ cm is measured across the canyon at the 1-cm isobath, while $L_c = 31.5$ cm is measured perpendicularly to W_c from the canyon head to the 0-cm isobath at the mouth.

Buoyant water was pumped from a separate reservoir by an Ismatec pump through a pipe with holes at the end located just below the free surface. A sponge covered the end of the pipe to minimize mixing between the buoyant water, which had a density ρ, and the ambient water of constant density ρ_a. A Plexiglas wall was placed next to the source to stop the growth of the bulge region and to force the flow to propagate along the wall. Density, expressed as a reduced gravity, $g' = g(\rho_a - \rho)/\rho_a$, where g is the acceleration due to gravity, was measured before each run and ranged from 4 to 23 cm s^{-2}. Pump rates, Q, were varied between each experiment as well and ranged from 4 to 23 cm^3 s^{-1} (Table 1).

An analog video camera mounted on the rotating table recorded each experiment from above. Visual observations were facilitated by dyeing the buoyant water and seeding the flow with surface particles. These video data were then converted to digital images at one frame per second.

Each experiment was run as follows: The tank was filled with ambient water and spun up to solid body rotation. Then the pump was turned on and the dyed buoyant water initiated the current from the source region. At first, a bulge formed around the source region, but its growth was stopped by the Plexiglas enclosure, and buoyant water propagated along the wall toward the model bathymetry (Fig. 3). Particles were placed on the surface of the flow by hand continually throughout the experiment. The flow was allowed to evolve until the current propagated past the bathymetry and around the entire rest of the tank, where it then started to interfere with the source region. In all cases, the experiments lasted long enough to allow a quasi-steady state to be reached.

b. Observing the laboratory flow

A two-step method was developed to characterize the flow field objectively. The first step was to define when

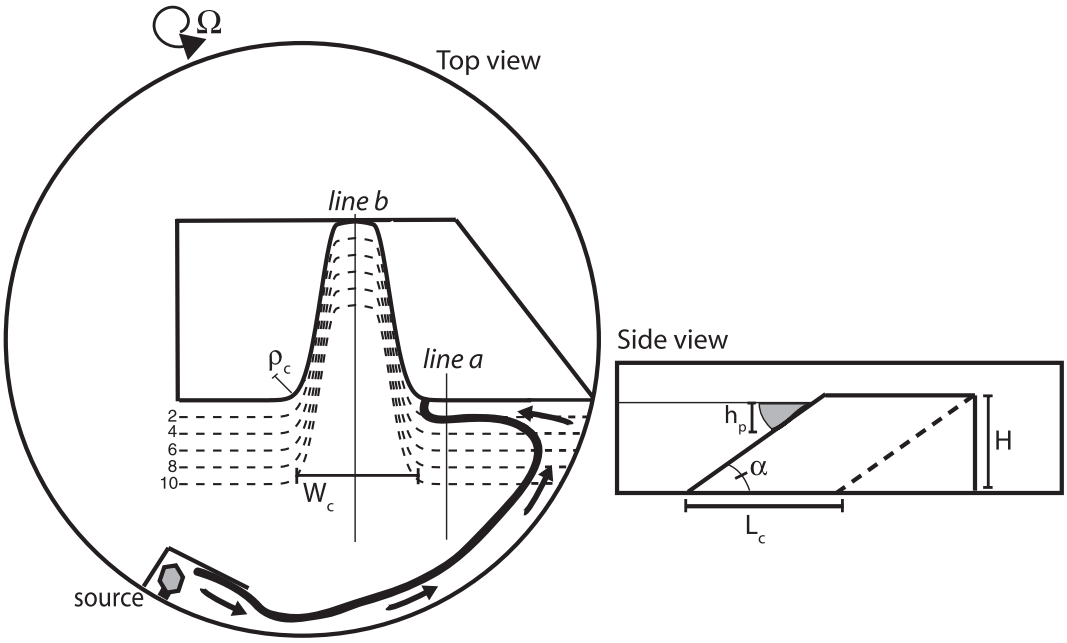

FIG. 3. (left) Top view of the laboratory setup. The arrows illustrate the path of the buoyant water from the source region, along the tank wall, and onto the sloping bathymetry, shown by dashed isobaths every 2 cm. (right) Side view of the laboratory setup. Solid lines show the bathymetry along line a, while the dashed line indicates the bathymetry inside the canyon along line b. The buoyant current is shaded gray and flows into the page.

the flow reached a quasi-steady state (see definition in section 4) after an initial transition phase. Then we quantified the flow field by looking at the position of the front along a line perpendicular to the head of the canyon (line b, Fig. 3). Figure 4 illustrates the two methods used to determine the position of the front. Using a particle- tracking software package in MATLAB, we identified the location of the particles at a certain time (Fig. 4a) and then used successive images to follow the particle trajectories throughout a certain time range. Since the particles traced the velocity signal, they also were indicators of the front location at the surface. The majority of particles were clustered near the maximum velocity of the current. Note that the maximum velocity does not correspond to the offshore edge of the buoyant current but is centered over the sloping interface between the buoyant water and the ambient water, as shown in Fig. 4a. The offshore distance from the coast to the location of the current maximum velocity was calculated for 20-s ranges for each run, along both lines a and b. We define this distance for line b as W_{obs}. The particle-tracking method was also used to calculate the surface current velocities upstream of the canyon (outlined region in Fig. 4a) before the influence of the bathymetric bend but after the current had equilibrated on the sloping bottom. Velocities at other depths and locations were not measured.

The second method to determine the frontal position used the intensity of the dye in the current (correlated to the current depth) as a proxy for the position of the foot of the front (Fig. 4b), defined as the location where the current front intersects the bottom at a depth h_p (Fig. 4b). We calculated the position of the foot of the front from the dye-intensity images along both lines a and b using 20-s bins, and those compare well to the particle-derived frontal positions. However, at later times, when the current was separated from the canyon slope, the dye method broke down due to corruption of the intensity images by reflections off the bottom of the tank. Thus, the dye method was used only to determine the starting time when the current first passed line b. Visual observations of the depth of the current were also facilitated by the dyed water. Throughout the rest of the paper, however, we use W_{obs} as calculated from the particle-tracking method.

4. Results

In all 14 experiments, the buoyant current propagated along the tank wall from the source region until it encountered the slope area (Fig. 3). Upon reaching the sloping bathymetry, the current slowed and widened, in accordance with previous laboratory experiments (Lentz and Helfrich 2002). Moving along-slope upstream of the

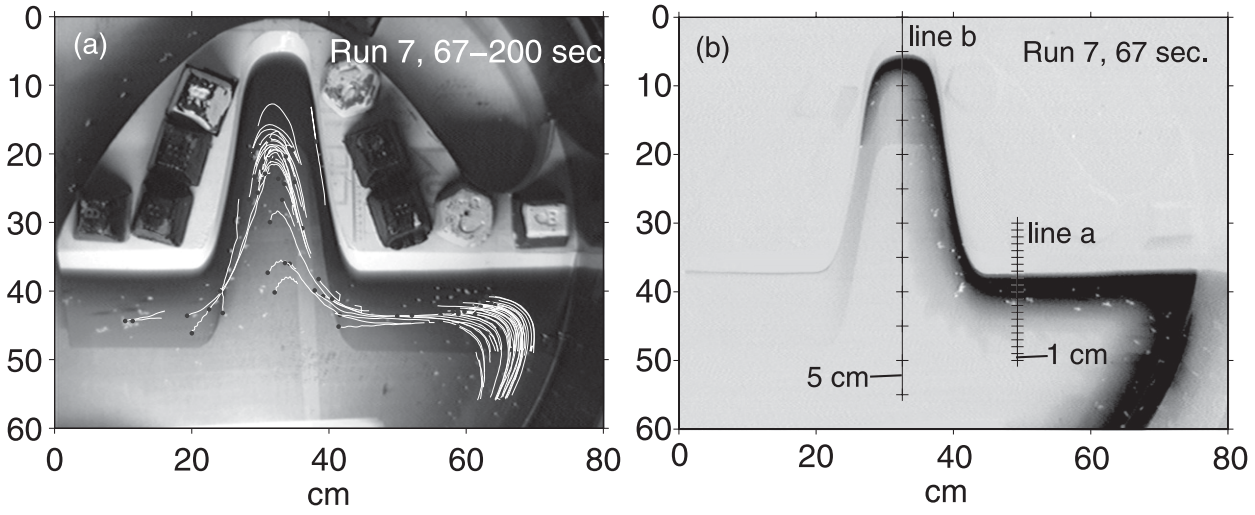

FIG. 4. (a) Top view of run 7 from a video frame over an arbitrary time period, which illustrates the particle tracking method. Black dots show the end position of each particle track. (b) Grayscale image of run 7, obtained at the starting time of (a), showing the buoyant current location using the dye as a proxy.

canyon, the flow equilibrated and the foot of the front approached h_p before the flow encountered the canyon.

Along line a, the current width scaled with the total predicted width, W, although a slow widening of the current throughout each run was also observed. In previous laboratory experiments (e.g., Lentz and Helfrich 2002), the width of the buoyant current grew in time like $t^{1/2}$, a process thought to be caused by entrainment due to interfacial drag. However, at line b the flow exhibited a different behavior (Fig. 5). During the early stages of each run, the width of the current inside the canyon, W_{obs}, increased rapidly for some time (Fig. 5a), then slowed to widen at a similar rate ($\sim t^{1/2}$) as the current on the upstream slope. This suggests that the current goes through a transition phase, with a rapid widening inside the canyon, until it reaches a quasi-steady state. The beginning of the quasi-steady state for each run was defined to be when $\partial W_{\text{obs}}/\partial t$—the slope of each line in Fig. 5—was reduced to $1/e$ of its maximum value attained during the transition phase.

In Fig. 5b, W_{obs} is scaled by L_c, the length of the canyon, so that $W_{\text{obs}}/L_c \sim 1$ indicates that the front moved offshore all the way to the canyon mouth. Time is scaled by $t_{\text{fill}} = Ah_p/kQ$, where A is the horizontal area within the canyon out to the position where the width of the canyon equals $2W$. Here kQ represents the percentage of inflow that does not exit the canyon region defined by A. The value of k was found by assuming $t/t_{\text{fill}} = 1$ at the start of the quasi-steady state of each run. The best fit for k for all the runs gives $k \approx 0.23$. The time scale t_{fill} represents the time it would take the buoyant current to fill up the volume Ah_p. Note that not all quasi-steady phases started exactly at $t/t_{\text{fill}} = 1$, owing to two possible factors. First, the position where the width of the canyon equals $2W$ may not correctly represent the location of the front in the canyon, as also suggested in section 5. Second, the percentage of inflow that does not exit the canyon region, kQ, is probably dependent on the dynamics of the flow and the different regimes discussed below. However, given the approximation in the scales used, the scatter about unity is small.

The current velocity, u_{obs}, was measured at line a during two periods for comparison (Fig. 6). Figure 6a shows that the velocity of the current, even at an initial time, was much less than c_w and that the speed decreased as each experiment progressed. During the initial time, the average $u_{\text{obs}}/c_w = 0.41 \pm 0.09$ (± 1 standard deviation). The decreasing flow speed is in agreement with previous laboratory experiments and is expected for a continually widening current (Lentz and Helfrich 2002). Using c_p instead of c_w, which takes into account the sloping bottom, results in an average $u_{\text{obs}}/c_p = 0.78 \pm 0.15$ at the initial time (Fig. 6b). Again, though, as the experiment progresses the flow slows down considerably with $u_{\text{obs}}/c_p = 0.55 \pm 0.11$.

a. Overview of the steady circulation: Three cases

By examining the quasi-steady states of all the runs, we found that we could replicate the flow separation positions found numerically by DC03. Depending on how far the buoyant current penetrated into the canyon, a distinct accompanying circulation was set up in the head of the canyon between the main part of the current and the canyon wall. These circulations are most likely

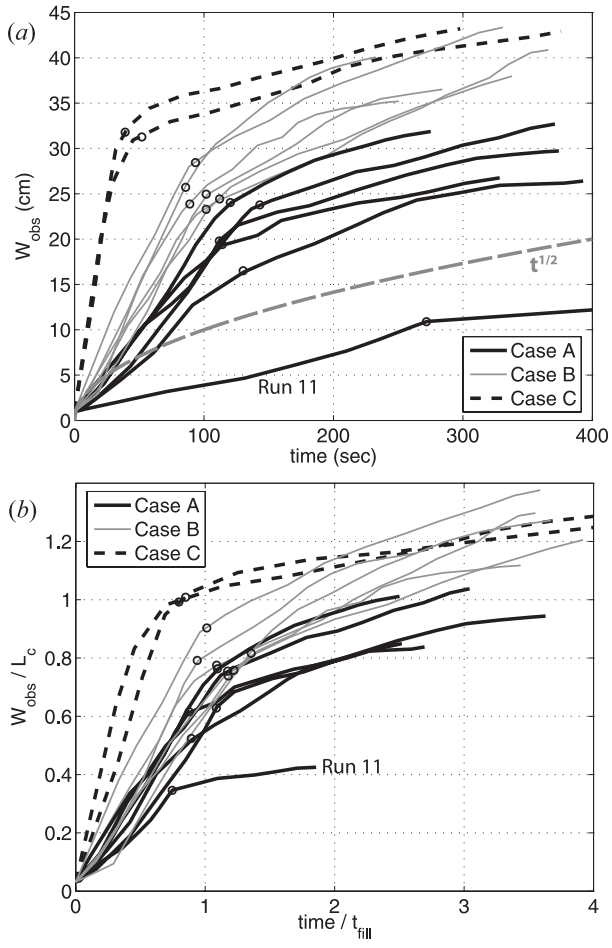

FIG. 5. (a) Current width W_{obs} as a function of time. The three cases, A–C, are differentiated by line type. Open circles mark the beginning of the quasi-steady state for each run. (b) As in (a) but the current width is normalized by the length of the canyon L_c and time is normalized by the filling time t_{fill}. A value of $W_{obs}/L_c = 1$ indicates that the front has moved offshore all the way to the canyon mouth.

related to the processes noted by previous studies on coastal current separation past a bathymetric feature, such as the gyre formation in the Alboran Sea (Bormans and Garrett 1989) or past Tsugaru Strait east of Japan (Kawasaki and Sugimoto 1984).

Figure 7 illustrates schematically the three cases observed. Note that each case in Fig. 7 is representative of the flow field at the start of the quasi-steady-state period: all of the analysis to follow uses data obtained from that specific time. The three circulations differ in the amount of penetration into the canyon by the buoyant current as well as in the details of the circulation created in the head of the canyon.

Case A is the ''no eddy'' case (Fig. 7a) in which the buoyant current was observed to follow the bathymetry farthest into the canyon with no separate circulation in the head of the canyon. Six experiments fell into this category (Table 1), and, although the exact position of the front along line b varied, no particles were observed to cross the canyon mouth in any of these runs.

In Case B, the ''one eddy'' case (Fig. 7b), the buoyant current did not penetrate as far into the canyon as in Case A. In these experiments, the final position of the front was observed to vary from midway in the canyon to near the canyon mouth. These runs also exhibited a closed anticyclonic circulation at the head of the canyon. This eddy feature formed during the transition phase as part of the current separating from the canyon slope turned to the right to form an anticyclone. Once the quasi-steady phase was reached, the anticyclone was isolated from the main part of the current. The separating part of the current flowed across the canyon and reconnected to the slope on the other side of it, continuing on to exit the canyon (Fig. 7b).

Case C runs (Fig. 7c) were characterized by an almost total separation of the current from the slope as soon as it encountered the canyon. Two distinct circulations were set up in the head of the canyon during the transition phase of Case C runs. Similar to Case B, an anticyclone formed just downstream of the separation point. However, as discussed in the next section, the deformation scale of the current limited the size of the anticyclone that was trapped to the upstream canyon wall. Flow that circuited around this anticyclonic eddy then split, either moving back toward the mouth of the canyon (thick red line, Fig. 7c) or continuing on cyclonically around the canyon head (thick closed line, Fig. 7c). This cyclonic flow then exited the canyon at the downstream bend and rejoined the part of the current that passed directly across the mouth. The flow across the mouth was the dominant pathway observed in these runs after the quasi-steady state was reached, although the current had a slight curvature into the canyon (Fig. 7c).

b. What controls the separation process?

As noted earlier, the behavior and scales of the buoyant current along the initial slope, line a in Fig. 3, were in good agreement with the extensive study of Lentz and Helfrich (2002). The focus of this section is on examining the dependence of the flow separation process on these scales, which are set along the initial slope upstream of the canyon. Tables 1 and 2 list the relevant scales for each flow behavior observed. Also listed in Table 2 is c_w/c_α varying from 0.1 to 2.7, which is much lower than the DC03 range of 3–18 but does span the two limits of c_w/c_α corresponding to the surface-trapped ($c_w/c_\alpha < 1$) and slope-controlled cases ($c_w/c_\alpha > 1$).

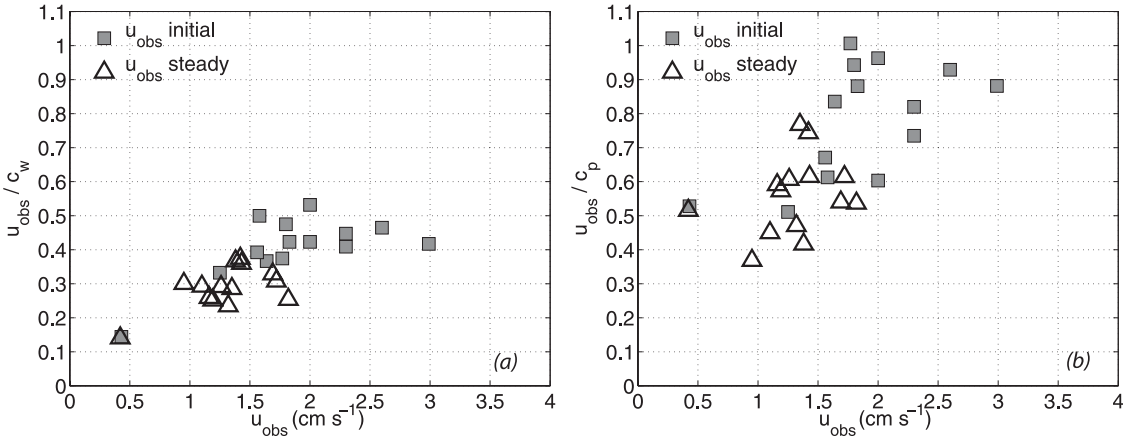

FIG. 6. (a) Observed speed of the buoyant current $u_{\rm obs}$ on the upstream slope (line a) at an initial time (gray squares) and at the start of the quasi-steady phase of each run (open triangles) vs $u_{\rm obs}$ normalized by the theoretical speed c_w. (b) As in (a) but for $u_{\rm obs}$ normalized by the propagation speed of the current, c_p.

The runs with the greatest penetration into the canyon (Case A) took the longest time to reach a steady state (Fig. 5a); that is, the front moved offshore the slowest during the transition phase of these runs. By contrast, the two Case C runs progressed relatively rapidly through the transition period. One experiment, run 11, behaved anomalously compared with the other runs with no fast growth inside the canyon (Fig. 5). Run 11 had the smallest reduced gravity and flow rate, which resulted in a relatively slow and narrow current; this might account for the observation that it seemed to grow like $t^{1/2}$ at all times.

The position $W_{{\rm obs},s}$ of the front at the beginning of the quasi-steady state (open circles, Fig. 5a) for each run is illustrated in Fig. 8a, which shows a clear dependence of the degree of separation, defined as $W_{{\rm obs},s}/L_c$, on the ratio W/ρ_c. Run 11, as noted above, displayed the least separation with $W_{{\rm obs},s}/L_c \sim 0.33$. The critical W/ρ_c value, above which the flow moves across the canyon mouth, is ~ 1, in agreement with previous studies in which separation occurred for $u/f\rho_c > 1$ (Bormans and Garrett 1989; Klinger 1994a). We chose not to use $u_{\rm obs}$ to estimate $u/f\rho_c$ because the current velocity decreased continuously during each run due to the widening of the current (Fig. 6). The inertial scale u/f is interpreted here as W, although the exact equivalence occurs only for surface-trapped flows. The separation point of the current from the canyon slope was farthest toward the mouth in Case C, which had widths larger than ρ_c.

Another way to look at the degree of separation of the buoyant current from the canyon slope is to examine the angle of the current, θ, as it enters the canyon (Fig. 8b). The angle of the current is calculated from the position of the front edge at line a to the front edge at line b (Fig. 4a). Larger angles indicate more penetration into the canyon, while $\theta = 0$ corresponds to a flow straight across the mouth. This figure emphasizes that even though the majority of the flow in Case C did not enter the canyon, part of the flow was distorted by the bathymetry. In a set of laboratory experiments investigating a surface current encountering a sharp corner in a two-layer system, Klinger (1994b) found that anticyclonic eddies were generated when the angle of the current was greater than or equal to 45°. This compares favorably to the data in Fig. 8b since the two cases (Cases B and C) with flow separation coincided with anticyclonic eddy generation inside the canyon.

For comparison, three runs of DC03 that spanned a similar range of flow separation behaviors as we observed in the laboratory are also plotted in Fig. 8. The general trend is the same: As the width of the current increased relative to the bathymetric radius of curvature, the location where the current separated from the canyon slope moved closer to the canyon mouth (i.e., $W_{{\rm obs},s}/L_c = 1$). The critical value of W/ρ_c from the present laboratory results and the model results are similar.

The condition for separation derived by DC03 requires that the bottom velocity in the alongfront direction goes to zero. Hence, indirect comparisons between the studies are necessary since a precise measurement of the bottom velocity of the current would have been challenging in the laboratory. It is important to note that in the DC03 model, flow separation occurred for all inflow parameters (i.e., all g' and Q) if the background current was absent. In the laboratory, no background current was present, but separation did not always occur. Thus, the separation process that we observed in these experiments differed somehow from those in DC03.

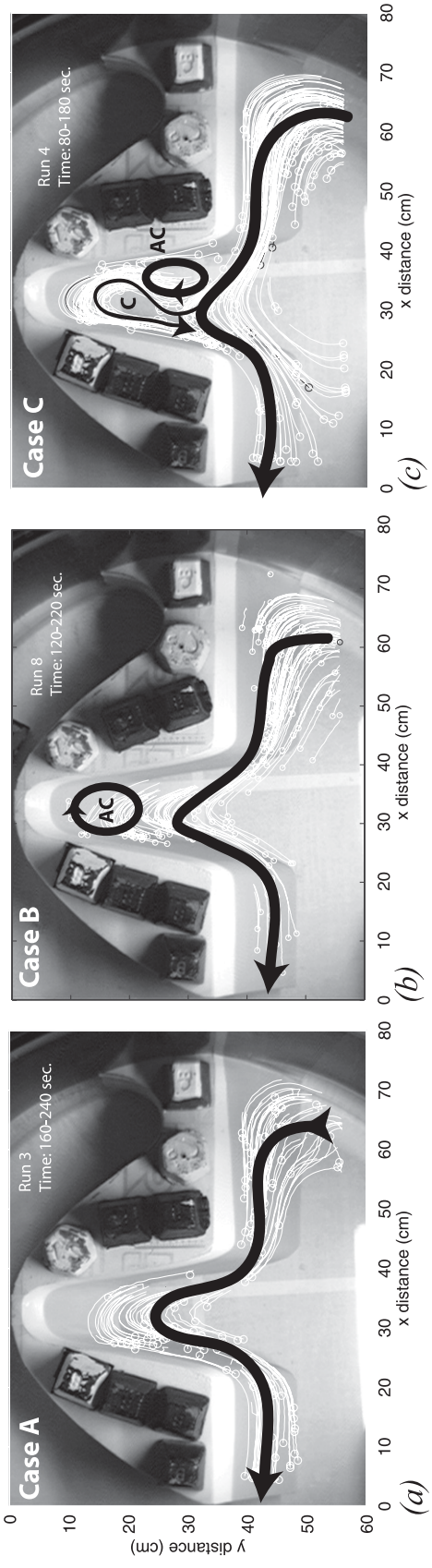

FIG. 7. Schematic of the three flow patterns observed (wide dark lines with arrowheads) overlaid on actual particle tracks from selected runs of each case. The three types are (a) Case A in which the greatest penetration into the canyon was observed along with no recirculation; (b) Case B with an intermediate penetration into the canyon and one anticyclonic (AC) eddy formed; and (c) Case C with the current separating across the canyon mouth, one anticyclonic eddy formed just past the separation point, and a cyclonic recirculation (C) in the canyon head.

TABLE 2. List of the relevant parameters observed to control the buoyant current behavior in the laboratory compared with the previous study of DC03 and with values derived from observations of the EGC/EGCC system.

	Bu (W/W_c)	W/ρ_c	c_w/c_a	Flow across canyon[a]
Case A	0.18–0.21	0.7–0.8	0.6–2.7	No: none to slight
Case B	0.21–0.26	0.9–1.1	0.5–1.3	Yes: midway up canyon
Case C	0.31–0.34	1.3–1.4	0.1–0.2	Yes: at mouth
DC03[b]	0.4–0.5	0.9–1.1	3–18	Yes: whole range observed
Ocean[c]	0.3–0.7	0.5–1.2	1.8–13	Yes: whole range suggested

[a] For the laboratory and DC03 this is for flow during the quasi-steady state of each run.
[b] Ranges taken from DC03 model results.
[c] Ranges taken from available observations of the EGC near the KG region.

Furthermore, in the real ocean the presence of stratification can decouple a buoyancy-driven current from the bottom if the current is surface trapped, adding another complication to determining whether a given flow will separate. For slope-controlled flows, the presence of stratification may affect the stability of the front separating the buoyant water from the ambient shelf water more than the separation process of the current.

We found a weak dependence of the flow behavior, characterized by the nondimensional current width in the canyon, on c_w/c_α (Fig. 9). The surface-trapped currents separated from the canyon slope closer to the canyon mouth, while the slope-controlled currents tended to follow the bathymetry far into the canyon. However, for intermediate values of c_w/c_α, close to 1, the flow exhibited a wide range of behaviors. As the ratios W/ρ_c and c_w/c_α can be calculated a priori, it is theoretically possible to fill in the missing parameter space in Fig. 9. Due to the limitation of using only one geometry (i.e., fixed W_c, ρ_c, and s) in the laboratory, it was not possible to set up runs with $c_w/c_\alpha \gg 1$ and $W/\rho_c > 1$ or to create surface-trapped currents ($c_w / c_\alpha \ll 1$) that had $W/\rho_c < 1$. In the present experiments, we believe that the parameter W/ρ_c controlled the degree of separation—not c_w / c_α since for the same value of c_w/c_α different levels of separation (i.e., $0.6 < W_{\mathrm{obs},s}/L_c < 1.0$) were observed. This result is also confirmed by the DC03 numerical runs in which slope-controlled currents can either separate from the canyon slope near the canyon mouth ($W_{\mathrm{obs},s}/L_c \sim 1$) or penetrate into the canyon ($W_{\mathrm{obs},s}/L_c < 1$). This further suggests that c_w/c_α is not the relevant parameter for the separation of a buoyant current from a canyon slope. Note that $W/\rho_c = \mathrm{Bu}W_c/\rho_c$ and in the present experiments W_c/ρ_c is a constant. Hence, Fig. 8 would be similar if Bu was used instead of W/ρ_c, with clearly a different interpretation

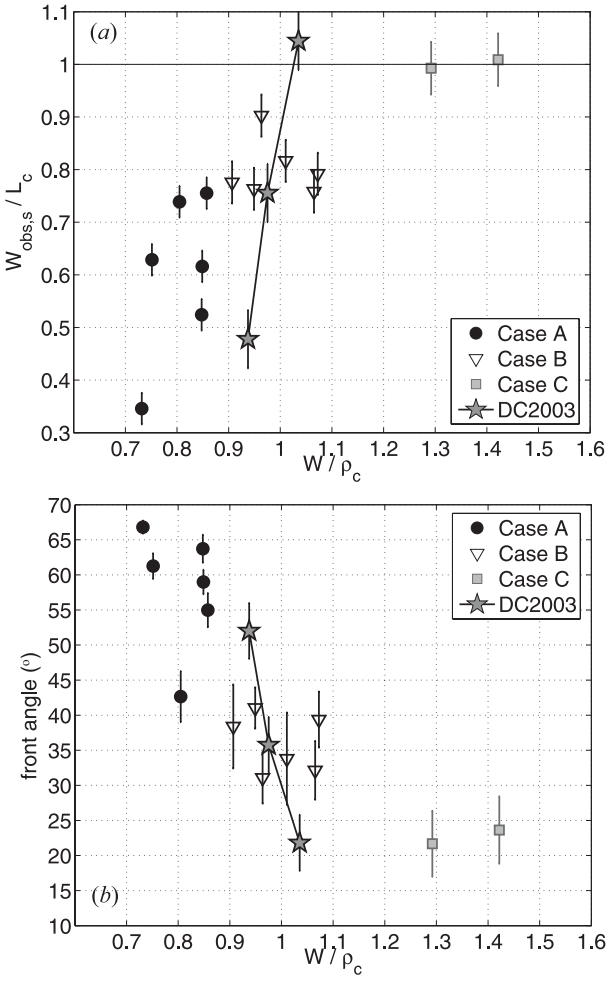

FIG. 8. (a) Plot of $W_{obs,s}/L_c$ vs the ratio of the predicted width of the current W and the radius of curvature ρ_c for laboratory results and DC03 model results (stars). A value of $W_{obs,s}/L_c = 1$ indicates separation of the current from the canyon slope at the canyon mouth. (b) As in (a) but for the angle θ of the current as it enters the canyon. Smaller angles indicate more flow straight across the canyon mouth.

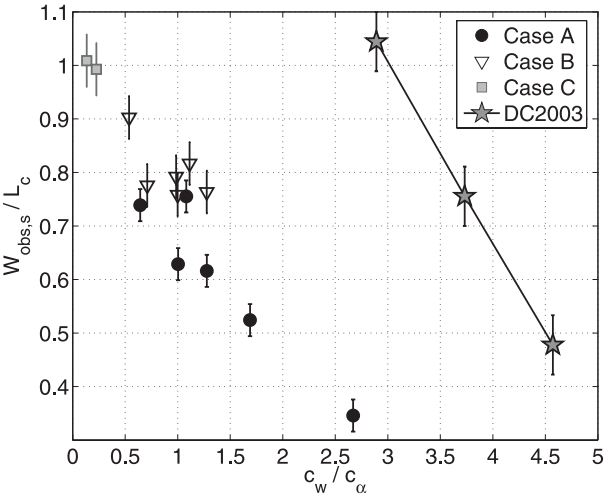

FIG. 9. Dependence of the nondimensional location of the buoyant current separation from the canyon slope, $W_{obs,s}/L_c$, on the degree to which bottom friction is important, indicated by c_w/c_α. Stars are taken from DC03.

of the results. Experiments with different geometries (i.e., different W_c and ρ_c) are necessary to be able to distinguish definitively between the dependence of $W_{obs,s}/L_c$ on Bu and W/ρ_c. However, as discussed in section 5, we believe that the formation of eddies in the canyon circulation supports our idea that the separation is controlled by W/ρ_c, a parameter found to determine eddy formation in the wake of bathymetric bends (e.g., Bormans and Garrett 1989; Klinger 1994b).

5. Discussion

The three cases of quasi-steady-state flow behavior described above span the range of flow separation behaviors observed in the laboratory. Case A was the simplest case (Fig. 7a) with the buoyant current entering and exiting the canyon without any portion of it moving across the mouth. All Case A runs had $W/\rho_c < 1$. This holds true even if the radius of curvature is increased to reflect the bathymetric curvature at the depth of the foot of the current. As no recirculation was observed in the head of the canyon in Case A but the position of the front inside the canyon varied slightly between runs (Fig. 8a), what then sets the quasi-steady-state position of the front? One potential explanation is the constraint of the canyon bathymetry on the current width itself. The quasi-steady-state position of the front inside the canyon should then scale with the position for which the canyon width is equal to $2W$. However, the present results do not support this hypothesis.

Flow separation was observed to occur in the Case B runs along the canyon slope region (Fig. 7b) along with the formation of an anticyclonic eddy in the head of the canyon. For these runs, W/ρ_c was near the critical value (Fig. 8) and the location of the buoyant current separation from the canyon slope was almost constant ($W_{obs,s}/L_c \sim 0.8$–0.9). The eddy formed as the separated current split upon hitting the downstream side of the canyon, creating two oppositely directed flows. Note that this is not a strong recirculation and could have been ignored (i.e., not shown in figures) in the numerical calculations of DC03 that showed flow separation. Similar closed circulations have been found in barotropic model runs (She and Klinck 2000) and in observations made in Astoria Canyon (Hickey 1997), both of which suggested that it was due to potential vorticity

conservation. Separation of the flow past the canyon bend was found to depend on the degree of momentum advection (She and Klinck 2000), which can be estimated by calculating a Rossby number $\mathrm{Ro} = u_{\mathrm{obs}}/fW$. In the present study, Ro ranged from 0.25 to 0.6 for Case A, 0.45 to 0.65 for Case B, and 0.8 to 0.9 for Case C, suggesting that large Rossby numbers are associated with separation.

The runs of Case C were similar to Case B but with complete separation of the current at the mouth of the canyon, confirming the validity of the $W > \rho_c$ criterion for separation to occur. The closed anticyclonic recirculation was constrained to hug the upstream canyon wall, which allowed a pathway for the current to move cyclonically through the head of the canyon and back out (Fig. 7c). As the current separated near the initial bend in the bathymetry, the flow in the eddy did not reach the downstream canyon wall and, instead, continued to rotate and turn back to split on the upstream canyon wall. Thus it fed both the cyclonic throughflow and the anticyclonic eddy that had a flow back toward the canyon mouth. The size of the anticyclonic eddy scaled with W_d.

Oceanographic relevance

Two hydrographic and velocity sections, one upstream and one downstream of the KG (Fig. 1), suggest that a variable pathway exists for the EGC around the KG region (Sutherland and Pickart 2008). To apply the laboratory results to the EGC system near the KG, we calculated the reduced gravity and depth of the EGC upstream of the KG from these hydrographic data. To calculate g' we used the difference between the average density over the shelf (ρ_a) and the average density within the EGC core (ρ). Those values were used to find the range of Bu, W/ρ_c, and c_w/c_α listed in Table 2.

The Kangerdlugssuaq Trough is a large canyon (width ~50 km) that crosses the entire shelf with depths up to 600 m, while typical shelf depths are ~250 m in this area. Since the KG canyon width and radius of curvature vary with depth, their values are selected at the depth of the foot of the front, h_p, that is, as a function of g' and Q (1). For example, ρ_c varies from a minimum of ~25 km on the 350-m isobath (Fig. 1) to ~40 km on the 250-m isobath (and to infinity if the current is over the continental slope, which continues straight down the Greenland coast). The radius ρ_c also depends on the smoothness of the bathymetry data used to estimate it, as arbitrarily small radii can be obtained with finescale bathymetric data. To get the values listed here we smooth the GEBCO bathymetric data (BODC et al. 2003) with a 2D filter that has a length scale of one Rossby radius.

The values of W/ρ_c for the EGC are within the parameter ranges of Case A and Case B, suggesting that, indeed, the EGC is susceptible to both moving across the KG as well as flowing into the canyon. It is instructive to ask what changes in the variables g', ρ_c, or h_p are needed to move W/ρ_c into a different regime. For example, observations in 2004 from north of Denmark Strait showed the EGC core to have $g' \sim 0.024$ m s^{-2}, $h_p \sim 300$ m, and $\rho_c \sim 22$ km so that $W/\rho_c = 0.9$, which is in the lower range of Case B. An increase in g' to 0.103 m s^{-2} (e.g., due to a surge in ice melt or surface heating) is required to make $W/\rho_c = 1.3$ and fit into Case C, where full separation is expected. On the other hand, a decrease in h_p to 275 m would lower W/ρ_c to 0.81, with the buoyant current predicted to flow toward the coast along the canyon slope. This suggests a likely seasonal effect to the splitting process of the EGC, in addition to the higher-frequency changes induced by the winds, for example.

The hypothesis that the EGC has a two-branch structure was first hinted at by a set of joint Icelandic–Norwegian cruises (Malmberg et al. 1967), which suggested that the EGCC is first found inshore near the KG area. Since then, hydrographic observations have shown distinct EGCC and EGC jets downstream of the KG, but with *T/S* characteristics in both currents similar to those in the EGC north of Denmark Strait (Sutherland and Pickart 2008). Other evidence illustrating the two-branch structure of the EGC in this area include an XCTD section taken across the KG (Fig. 1), which found a recirculation within the canyon of Atlantic-influenced water from the Irminger Current present on both sides of the canyon (Sutherland and Pickart 2008). Also, velocities derived from drifters indicate two distinct jets downstream of the KG where the EGCC/EGC system navigates around the Sermilik Trough (ST) (Fig. 1; Jakobsen et al. 2003; Centurioni and Gould 2004). Finally, satellite-derived sea ice concentrations commonly show a large-scale meander curving toward the coast near the KG (Cavalieri et al. 2005).

If we assume that the EGC does flow toward Greenland along the KG canyon, what is the process that causes the EGCC to form as a distinct flow instead of the EGC returning unaltered back to the shelf break? A possible scenario relies on the effects of mixing and the fact that the isobaths diverge on the downstream side of the Kangerdlugssuaq Trough near the head of the canyon (Fig. 1). Mixing of the buoyant polar-origin EGC water with the Atlantic-influenced water of the Irminger Sea, which is brought into the canyon as the Irminger Current turns toward Greenland, would reduce the buoyancy of the current. This decrease in g' would reduce the trapping depth of the current (h_p) so that it could exit

the canyon on a shallower isobath, that is, as the EGCC. For example, the 200-m isobath near the head of the KG starts out toward the shelf break but turns abruptly about a quarter of the way out back toward the coast (Fig. 1). Observations of the EGCC farther downstream suggest that it is trapped to isobaths in the range 100–200 m (Wilkinson and Bacon 2005; Sutherland and Pickart 2008).

Numerous other processes further complicate the circulation over the Greenland shelf. In particular, the effect of the wind on the EGC and EGCC is strong (Sutherland and Pickart 2008) and, for a surface-trapped flow, it could exert a dominant influence on the path of the current. In general, the winds in this area are northeasterly (downwelling favorable). These strong wind events might have a profound influence not only on the upper layer flow behavior (i.e., EGC separation or not) but also on the amount of cross-shelf exchange between the lower layers of the canyon and offshore water (e.g., Castelao and Barth 2006; She and Klinck 2000; Allen et al. 2003). The influence of ice advection/formation on this effect in winter is unclear but probable.

The area downstream of Denmark Strait, including the KG, is also known to be a site of high eddy kinetic energy (e.g., Jakobsen et al. 2003; Centurioni and Gould 2004). What effect these eddies have on the separation of the EGC is unknown, but the cross-shelf exchange of warm/salty water from offshore with the polar-origin EGC would certainly enhance any effects due to mixing. Tidal currents are generally small in the Nordic and Irminger Seas, but can reach up to 20 cm s^{-1} over the shelf near the KG (Sutherland and Pickart 2008). The effects of tidal currents on mixing between the EGC and Irminger Sea Water, and the strength of the EGC and its interaction with the KG, are unknown.

The results found here could also be applied to other regions of the EGC/EGCC system. One important area might be Cape Farewell, at the southern tip of Greenland since, if the EGC and EGCC were to separate there, the buoyant water might influence the stratification of the interior water and thus the degree of convection that might occur in the Irminger Sea (Holliday et al. 2007). However, $\rho_c \geq 90$ km for Cape Farewell and is much greater than the local maximum Rossby radius of deformation, so separation is not likely. Wind and bathymetric effects are more probable candidates for the offshore movement of the EGCC observed near Cape Farewell (Holliday et al. 2007; Sutherland and Pickart 2008).

6. Summary

The circulation over the southeast Greenland shelf and slope is dominated by an equatorward-flowing buoyant current system but is complicated by the presence of irregular shelf bathymetry, strong along-shelf winds, and significant eddy activity. This study presented a set of laboratory experiments focused on what controls the separation of a buoyant current interacting with a canyon.

We observed a range of flow behaviors that were time and scale dependent and in agreement with previous studies. The separation of the buoyant current at the upstream edge of a canyon was found to depend on the current width relative to the radius of curvature of the topography. The flow moved across the mouth of the canyon when the ratio $W/\rho_c > 1$. Accompanying the buoyant current separation was the creation of an upper- layer circulation inside the canyon; these recirculations fit into three categories characterized by the location of the separation point. The simplest case showed no recirculation in the head of the canyon and no flow separation, while the other two cases showed eddy features that formed in the lee of the separating current.

There are several important distinctions between the present laboratory experiments and the studies examined previously. First, the present laboratory flows spanned a wider range of currents with both slope-controlled and surface-trapped flows as well as using a geometry more relevant to buoyant current–canyon interaction. In the intermediate range of c_w/c_α (close to 1), currents were observed to both separate completely and not separate at all, suggesting that, although bottom friction is important in determining the location of the front, separation driven by the inertia of the flow could overcome even the strongest bathymetric influence. A second difference is that, although no background current was present, separation did not always occur, in contrast to the model results of DC03. Finally, the focus here was on the buoyant current system, while the majority of previous studies looked at barotropic flow fields with constant stratification.

The present results support the hypothesis that the East Greenland Current may separate at the Kangerdlugssuaq Trough canyon, as the range of oceanic values of W/ρ_c span those in the laboratory in which both separation and no separation were observed. What causes the EGCC to form as a distinct jet downstream of the canyon is still unclear but is possibly due to mixing within the canyon or to bathymetric steering at the head of the canyon, where some of the isobaths diverge and follow an inshore route (the EGCC) or a shelfbreak route (the EGC recirculation). The temporal variability of this process likely occurs on time scales of days to weeks since the strength of the EGC can vary significantly on these synoptic time scales and is most likely influenced by the significant eddy activity observed near the canyon.

Acknowledgments. This work was partially funded by NSF Grant OCE-0450658. DS also received support from the Academic Programs Office of the Woods Hole Oceanographic Institution, while CC had partial support from NSF OCE-0350891. The authors thank Keith Bradley for help in constructing the laboratory setup, Bob Pickart for the generous use of his data, and Steve Lentz and Carlos Moffat for useful comments. The comments of two anonymous reviewers were greatly beneficial in clarifying the motivation and conclusions of this paper.

REFERENCES

Allen, S. E., M. S. Dinniman, J. M. Klinck, D. D. Gorby, A. J. Hewett, and B. M. Hickey, 2003: On vertical advection truncation errors in terrain-following numerical models: Comparison to a laboratory model for upwelling over submarine canyons. *J. Geophys. Res.,* **108,** 3003, doi:10.1029/2001JC000978.

Bacon, S., G. Reverdin, I. G. Rigor, and H. M. Smith, 2002: A freshwater jet on the east Greenland shelf. *J. Geophys. Res.,* **107,** 3068, doi:10.1029/2001JC000935.

——, P. G. Myers, B. Rudels, and D. A. Sutherland, 2008: Accessing the inaccessible: Buoyancy-driven coastal currents on the shelves of Greenland and eastern Canada. *Arctic-Subarctic Ocean Fluxes: Defining the Role of the Northern Seas in Climate,* R. Dickson et al., Eds., Springer, 703–722.

BODC, cited 2003: The Centenary Edition of the GEBCO Digital Atlas. British Oceanographic Data Centre, digital media. [Available online at http://www.bodc.ac.uk/data/online_delivery/gebco/.]

Bormans, M., and C. Garrett, 1989: A simple criterion for gyre formation by the surface outflow from a strait, with application to the Alboran Sea. *J. Geophys. Res.,* **94,** 12 637–12 644.

Castelao, R. M., and J. A. Barth, 2006: The relative importance of wind strength and along-shelf bathymetric variations on the separation of a coastal upwelling jet. *J. Phys. Oceanogr.,* **36,** 412–425.

Cavalieri, D., C. Parkinson, P. Gloerson, and H. J. Zwally, 2005: Sea ice concentrations from Nimbus-7 SMMR and DMSP SSM/I passive microwave data, 2001–2004. National Snow and Ice Data Center, Boulder, CO, digital media. [Available online at http://nsidc.org/data/nsidc-0081.html.]

Cenedese, A., C. Vigarie, and E. V. di Modrone, 2005: Effects of a topographic gradient on coastal current dynamics. *J. Geophys. Res.,* **110,** C09009, doi:10.1029/2004JC002632.

Cenedese, C., and P. F. Linden, 2002: Stability of a buoyancy-driven coastal current at the shelf break. *J. Fluid Mech.,* **452,** 97–121.

Centurioni, L. R., and W. J. Gould, 2004: Winter conditions in the Irminger Sea observed with profiling floats. *J. Mar. Res.,* **62,** 313–336.

Chapman, D. C., 2003: Separation of an advectively trapped buoyancy current at a bathymetric bend. *J. Phys. Oceanogr.,* **33,** 1108–1121.

——, and S. J. Lentz, 1994: Trapping of a coastal density front by the bottom boundary layer. *J. Phys. Oceanogr.,* **24,** 1464–1479.

Cho, Y.-K., R. C. Beardsley, and V. A. Sheremet, 2002: On the cause of Scotian Shelf crossovers. *Geophys. Res. Lett.,* **29,** 2212, doi:10.1029/2002GL014968.

Garrett, C., 1995: Flow separation in the ocean. *Topographic Effects in the Ocean: Proc. 'Aha Huliko'a Hawaiian Winter Workshop*, Honolulu, HI, University of Hawaii at Manoa, 119–124.

Griffiths, R. W., and P. F. Linden, 1981: The stability of buoyancy driven coastal currents. *Dyn. Atmos. Oceans,* **5,** 281–306.

Hickey, B. M., 1997: The response of a steep-sided, narrow canyon to time-variable wind forcing. *J. Phys. Oceanogr.,* **27,** 697–726.

Holliday, N. P., A. Meyer, S. Bacon, S. G. Alderson, and B. de Cuevas, 2007: Retroflection of part of the east Greenland current at Cape Farewell. *Geophys. Res. Lett.,* **34,** L07609, doi:10.1029/2006GL029085.

Jakobsen, P. K., M. H. Ribergaard, D. Quadfasel, T. Schmith, and C. W. Hughes, 2003: Near-surface circulation in the northern North Atlantic as inferred from Lagrangian drifters: Variability from the mesoscale to the interannual. *J. Geophys. Res.,* **108,** 3251, doi:10.1029/2002JC001554.

Kawasaki, V., and T. Sugimoto, 1984: Experimental studies on the formation and degeneration processes of the Tsugaru Warm Gyre. *Ocean Hydrodynamics of the Japan and East China Seas,* T. Ichiye, Ed., Elsevier Oceanographic Series, Vol. 39, Elsevier, 225–238.

Klinck, J. M., 1996: Circulation near submarine canyons: A modeling study. *J. Geophys. Res.,* **101,** 1211–1223.

Klinger, B. A., 1994a: Inviscid current separation from rounded capes. *J. Phys. Oceanogr.,* **24,** 1805–1811.

——, 1994b: Baroclinic eddy generation at a sharp corner in a rotating system. *J. Geophys. Res.,* **99,** 12 515–12 531.

Lentz, S. J., and K. R. Helfrich, 2002: Buoyant gravity currents along a sloping bottom in a rotating fluid. *J. Fluid Mech.,* **464,** 251–278.

——, and J. Largier, 2006: The influence of wind forcing on the Chesapeake Bay buoyant coastal current. *J. Phys. Oceanogr.,* **36,** 1305–1316.

Malmberg, S.-A., H. G. Gade, and H. E. Sweers, 1967: Report on the second joint Icelandic–Norwegian expedition to the area between Iceland and Greenland in August–September 1965. NATO Subcommittee on Oceanographic Research Tech. Rep. 41, Irminger Sea Project, 44 pp.

Pickart, R. S., D. J. Torres, and P. S. Fratantoni, 2005: The east Greenland spill jet. *J. Phys. Oceanogr.,* **35,** 1037–1053.

She, J., and J. M. Klinck, 2000: Flow near submarine canyons driven by constant winds. *J. Geophys. Res.,* **105,** 28 671–28 694.

Sheremet, V. A., and J. Kuehl, 2007: Gap-leaping western boundary currents in a circular tank model. *J. Phys. Oceanogr.,* **37,** 1488–1495.

Sutherland, D. A., and R. S. Pickart, 2008: The East Greenland Coastal Current: Structure, variability, and forcing. *Prog. Oceanogr.,* **78,** 58–77.

Whitehead, J. A., and A. K. Miller, 1979: Laboratory simulation of the gyre in the Alboran Sea. *J. Geophys. Res.,* **84,** 3733–3742.

Wilkinson, D., and S. Bacon, 2005: The spatial and temporal variability of the East Greenland Coastal Current from historic data. *Geophys. Res. Lett.,* **32,** L24618, doi:10.1029/2005GL024232.

Williams, W. J., G. G. Gawarkiewicz, and R. C. Beardsley, 2001: The adjustment of a shelfbreak jet to cross-shelf topography. *Deep-Sea Res. II,* **48,** 373–393.

Wolfe, C. L., and C. Cenedese, 2006: Laboratory experiments on eddy generation by a buoyant coastal current flowing over variable bathymetry. *J. Phys. Oceanogr.,* **36,** 395–411.

Yankovsky, A. E., and D. C. Chapman, 1997: A simple theory for the fate of buoyant coastal discharges. *J. Phys. Oceanogr.,* **27,** 1386–1401.